JOURNAL OF MATERIALS SCIENCE 27 (1992) 5597–5602

Pressureless sintered ATZ and ZTA ceramic composites

R. CHAIM
Department of Materials Engineering, Technion – Israel Institute of Technology, Haifa 32000, Israel

Alumina–20 wt% zirconia (ATZ) and zirconia–20 wt% alumina (ZTA) composites were prepared by conventional sintering of commercial powders, with average particle sizes in the range 0.35–0.70 μm. Sintering at 1650 °C for 4 h resulted in final densities up to 96%. Bending strength and hardness increased with the final density. The tetragonal volume fraction was strongly dependent on both the final density and tetragonal grain size. The relatively high fracture toughness of 9 MPa $m^{1/2}$ was associated with the highly dense microstructure consisting of tetragonal grains of the critical size.

1. Introduction

Composites based on the ZrO_2–Al_2O_3 system – alumina-toughened zirconia (ATZ) and zirconia-toughened alumina (ZTA) – exhibit the highest mechanical performances observed for particulate ceramics [1–4]. (A thorough review was presented by Wang and Stevens [5].) This improvement in bending strength and fracture toughness was found to be achieved through distinct mechanisms. In the first case, the low proportions of zirconia grains make for improved strength by inhibiting alumina grain growth [6–10]. In the second, the mechanism consists in metastable retention of the tetragonal grains through chemical stabilization resulting from the limited alumina dissolution in the zirconia [11], as well as through the elastic constraint imposed by the alumina matrix on the zirconia grains [12, 13], with the attendant effects of transformation toughening and microcrack toughening [14–16].

In view of the technical problems associated with the dissimilar sintering behaviour of Al_2O_3 and ZrO_2 [17, 18], uniaxial or isostatical hot-pressing was often resorted to in preparing the composites, thereby facilitating achievement of the fine-grained high-density (close to the theoretical) product on which the improved mechanical properties are conditional [19, 20]. Accordingly, recent efforts centred on fine powders, in view of their superplastic behaviour at high temperatures [21–23].

The present paper describes the microstructures and corresponding mechanical properties in selective ATZ and ZTA composites, produced by conventional sintering from powders of varying original particle size.

2. Experimental procedure

2.1. Preparation of composite

Various grades of ZrO_2 and Al_2O_3 powders were used (except for the commercial ATZ powder (no. 5), which was received in mixed form). Compositions, phase contents, and average particle sizes as well as the sources are listed in Table I.

The powders were blended into mixtures with compositions ZrO_2 + 20 wt % Al_2O_3 (denoted ATZ) and Al_2O_3 + 20 wt % ZrO_2 (denoted ZTA), differing in average particle size. A slurry was prepared with deionized water (solid/liquid ratio 20%), wet ball milled (1 cm × 1 cm zirconia cylinders) for 24 h, and sampled for determining the particle-size distribution by sedimentation. At the final stage of the ball milling, 1% polyelectrolyte deflocculant (PC-85 Dolapix) and 5% polyvinyl alcohol (PVA) as binder were added. The slurry was then spread on the plaster board for drying and the resulting cast passed through a 30 mesh sieve (≃ 550 μm granules).

The powders were uniaxially cold-pressed at ≃ 200 MPa into 35 × 45 × 10 mm^3 compacts, which were heated to 400 °C, and kept for 1 h at that level for burn-out of the polymeric additives. The temperature was then raised (at a rate of 100 °C h^{-1}) to 1400 and 1650 °C, at which the samples were sintered for 6 and 4 h, respectively. The characteristics of the mixed powders, and the green and final densities of the samples (measured by Archimedes' suspension technique), are given in Table II.

2.2. Mechanical properties

The sintered plates were checked by the penetrant-liquid method ("filtered particles") for surface flaws or cracks, and those found flaw-free were cut for bending tests into 4 × 6 × 40 mm^3 bar specimens, whose edges were chamfered at 45° (with 25 μm removed). The specimens were polished lengthwise, using 600 grit SiC abrasive paper.

Fracture toughness, K_c, was determined by four-point bending of single-edge notched beam (SENB)

0022–2461

TABLE I Characteristics of the Al_2O_3 and ZrO_2 powders

Powder	Chemical composition	Designation[a]	Phase content[b] (%)			Average particle size d_{50}[c] (μm)
			t	m	Alpha	
Alumina powders						
1.	Al_2O_3 + 0.5 wt % MgO	A16	–	–	Alpha	0.50
2.	Al_2O_3 + 0.5 wt % MgO	AR1	–	–	Alpha	0.70
Zirconia powders						
3.	ZrO_2 + 5 wt % Y_2O_3	F5Y	50	50	–	0.35
4.	ZrO_2 + 4 wt % Y_2O_3	ZR1	30	70	–	0.70
ATZ powder						
5.	ZrO_2 + 4 wt % Y_2O_3 + 20 wt % Al_2O_3	SZ	90	10	Alpha	0.35

[a] Alcoa A16; AR1 and ZR1 Rami Special Refractories, Acco, Israel; F5Y Dynamit Nobel; SZ Toyo-Soda, Japan.
[b] Determined by XRD in the present study.
[c] Manufacturer's data.

TABLE II Composition, sintering conditions and density of the ATZ and ZTA samples

Sample	Powder particle size, d_{50}	Sintering conditions (°C/h)	Density (%)	
			Green	Final
ATZ-1	ZrO_2 (0.70 μm) + Al_2O_3 (0.70 μm)	1400/6	58	91
ATZ-2	ZrO_2 (0.35 μm) + Al_2O_3 (0.50 μm)	1650/4	52	95
ATZ-3	ZrO_2 (0.35 μm) + Al_2O_3 (0.35 μm)	1650/4	50	96
ZTA-4	Al_2O_3 (0.50 μm) + ZrO_2 (0.35 μm)	1650/4	54	94

specimens with 25 mm span, notched using a 0.15 mm thick diamond saw to a depth of $\simeq 0.30$ of the bar height.

All tests were carried out on an Instron model 1195 tensile machine, at crosshead velocity 0.1 mm min^{-1}. Flexural strength was determined by three-point bending of similar bars with 18 mm span.

Vickers hardness was measured on the polished surfaces at a 1 kg load, under which no cracks were observed around the indent.

2.3. Microstructural characterization

The microstructure of the samples was examined by scanning electron microscopy (SEM, JSM-840) and transmission electron microscopy (TEM, 2000-FX). SEM observations were performed either on polished and thermally etched samples, or on fracture surfaces coated with evaporated gold. TEM specimens were prepared by conventional methods of mechanical thinning and dimpling, ion milling to perforation, and finally coating with amorphous carbon.

The phase content of the samples was determined by X-ray diffraction (XRD). The diffractometer (PW-1820) was operated at 40 kV and 40 mA, using monochromatized (graphite) CuK_α radiation (scan speed 0.5° min^{-1}).

Grain size was determined from the TEM and SEM images by the line intercept method.

3. Results and discussion

3.1. Composite preparation

Typical sedigraphs of three slurries are presented in Fig. 1. The average particle size of the coarsest powders (ATZ-1) is seen to be almost doubled, from $d_{50} = 0.7$ μm in the original powders to $d_{50} = 1.45$ μm, presumably due to some agglomeration, and relatively wide particle-size distribution was observed. (By contrast, the as-received mixed powder (ATZ-3) which contained the finest particles, is characterized by its original narrow distribution, with $d_{50} = 0.35$ μm.) The distribution of the medium-size mixed powders (0.35 and 0.50 μm in various ratios) was consistent with the original particle sizes, as shown in the figure for the ZTA-4 slurry. Despite the wide distribution of the mixed powders, their average particle size of $d_{50} = 0.44$ μm is in good agreement with that expected for them. Thus, the medium-size mixed powders could be considered as agglomerate-free.

While the green density of the cold-pressed compacts increased at larger particle size and wider size distribution (Table II), the opposite trend was observed for the final density. For a given sintering regime (as exemplified by ATZ-2 and ATZ-3), the densification rate was higher in the case of the finer particles, probably due to the surface area contribution. These results indicate that as expected, higher close-packed compacts may be achieved with coarser

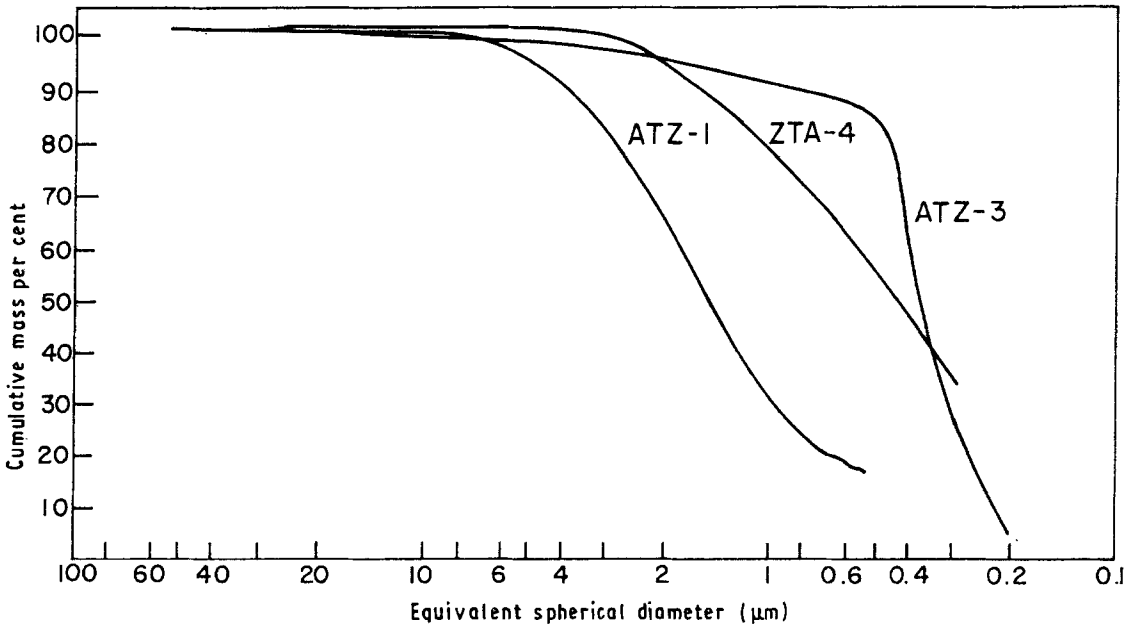

Figure 1 Typical sedigraphic data showing the cumulative size distribution of the mixed powder slurries.

TABLE III Mechanical properties and phase content of the ATZ and ZTA samples

Sample	K_c[a,b] (MPa m$^{1/2}$)	σ_b[b] (MPa)	H_v[c] (GPa)	Phase content (vol %)		Grain size range and average (μm)	
				t	m	Al_2O_3	ZrO_2
ATZ-1	5.5	250	8.7	50	50	0.36–1.30	0.14–1.10
	± 0.1	± 10				0.74	0.37
ATZ-2	5.6	300	13.5	88	12	–	–
	± 0.2	± 90					
ATZ-3	9.0	450	15.0	93	7	0.54–1.73	0.45–1.50
	± 0.5	± 50				1.86	0.91
ZTA-4	5.5	270	16.8	83	17	1.08–8.10	0.54–2.16
	± 0.5	± 30				1.80	1.38

[a] SENB method.
[b] Averaged over five test specimens.
[c] Accuracy of ± 0.2.

powders and a wider size distribution within the submicrometre range.

3.2. Microstructure

The volume fractions of the various zirconia polymorphs (cubic, tetragonal and monoclinic, c, t, m) present in the as-received powders were determined on the basis of the (1 1 1) and (4 0 0)-type reflections in the X-ray diffraction spectra. The quantitative analysis was based on the "polymorph method" equation as corrected by Porter and Heuer [24], and the results are shown in Tables I and III. No detectable cubic phase was found in the present samples. As could be expected, there is a direct correlation between the fine ZrO_2 particle size and high t-phase content in the zirconia powders (Table I). Most probably, the Al_2O_3 in the ATZ powder also acted as stabilizer for the t-phase [11].

The volume content of the t-phase in the sintered specimens (Table III), was found to depend both on the final density and on the t grain size. In the denser specimens (ATZ-2, ATZ-3 and ZTA-4), where sintering was followed by grain growth, the t-phase volume increased with decrease of the zirconia grain size. However, despite the fine zirconia grain size in ATZ-1, a high volume fraction of the m-phase was observed, and is attributable to the incompletely sintered microstructure of this specimen. These results bring out the two factors in the metastable retention of the t grains, namely the critical grain size and the elastic constraint of the surrounding matrix. TEM images revealed this effect in the ATZ-1 specimen in the form of numerous polyhedral pores (Fig. 2a), where the Al_2O_3 grains ("A" in the figure) are distinguishable by the presence of internal pores and some dislocations (in the larger grains), and many zirconia grains are twinned irrespective of their size (dark grains), indicating their m symmetry. In several regions, Al_2O_3 grain clusters were observed (Fig. 2b), and may be evidence of the agglomeration within the slurry referred to earlier (see Fig. 1). The average size

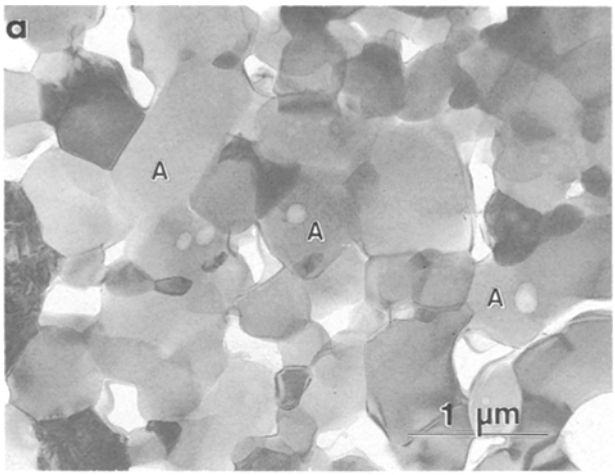

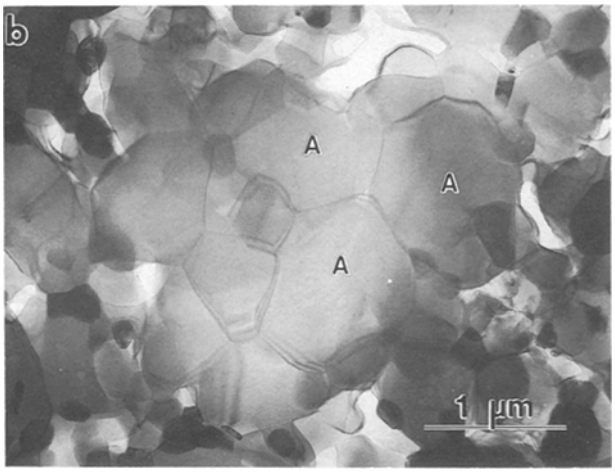

Figure 2 Bright-field transmission electron micrographs of the ATZ-1 specimen showing (a) homogeneous distribution of the alumina (A) and zirconia (dark) grains, (b) Al_2O_3 grain agglomerate left after ball-milling.

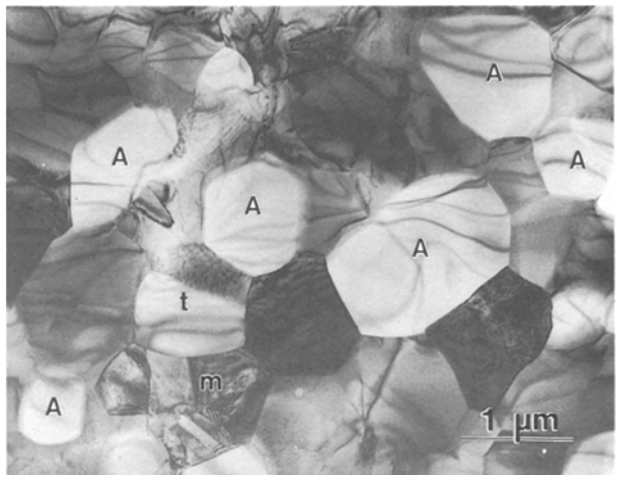

Figure 3 Bright-field transmission electron micrograph showing the homogeneously distributed alumina and zirconia grains, within the dense fine-grained ATZ-3.

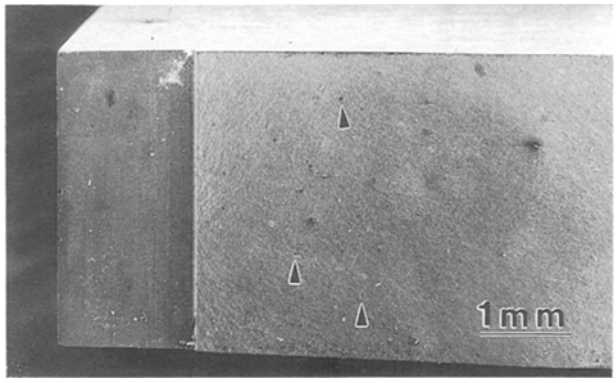

Figure 4 SEM image of the ATZ-3 fracture surface. The smooth fracture surface is evidence of the fine-grained dense composite. Some large voids present in the specimen are arrowed.

of these agglomerates is beyond a few micrometres, in agreement with the sedigraphic measurements.

The ATZ-3 specimen is characterized by the very dense and crack-free microstructure, in which submicrometre-size zirconia and alumina grains are uniformly distributed (Fig. 3). The Al_2O_3 grains are mostly defect-free and the zirconia grains have preserved their t-symmetry. In some cases the t grains were transformed under the TEM by the electron beam irradiation, which confirms their metastable nature. SEM fractography of this specimen revealed very smooth fracture surfaces, indicative of the highly dense material, but a few large pores were also observed (arrowed in Fig. 4).

The SEM image of the ZTA-4 specimen (Fig. 5) shows a relatively dense microstructure, with submicrometre zirconia grains uniformly distributed as inter- and intragranular particles in the alumina matrix grains. The intergranular grains are characterized by faceted surfaces, in contrast to the rounded shape of their intragranular counterparts. This microstructural change is indicative of the process in which zirconia grains were trapped within the growing alumina grains [25].

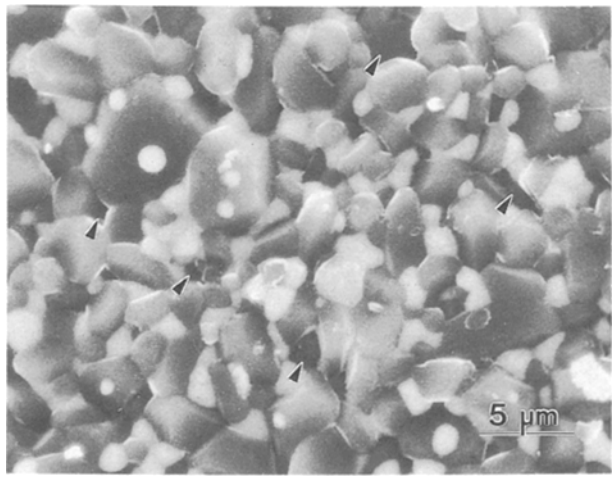

Figure 5 SEM image of thermally etched ZTA-4 specimen showing inter- and intragranular zirconia grains (white), within the alumina matrix grains. The arrows point to the porosities.

The ZTA-4 specimen shows in TEM submicrometre zirconia grains with either t- or m-symmetry, and larger alumina grains (Fig. 6). The latter were often found to be dislocated, as reported elsewhere in

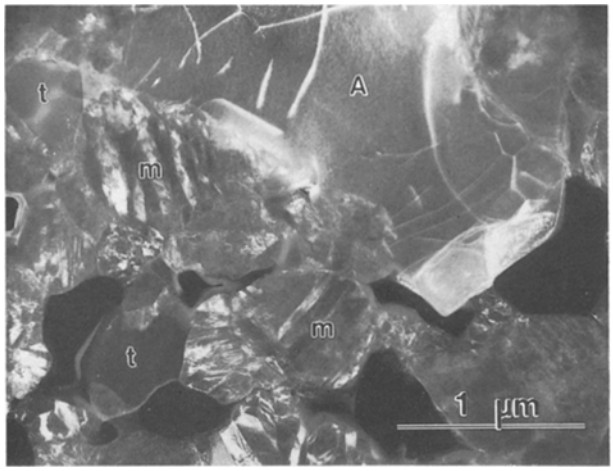

Figure 6 Dark-field transmission electron micrograph of the ZTA-4 specimen, showing the dislocation arrays in the large alumina (A) grains, and twins within the monoclinic (m) grains. The high porosity is an artefact due to specimen preparation by ion-milling.

cases involving transformed m-zirconia particles [9]. This phenomenon is most probably due to the ball milling, an explanation supported by the fact that the dislocation networks and arrays are associated with the larger rather than with the smaller grains.

3.3. Mechanical properties

The average fracture toughness, bending strength and Vicker's hardness results of the various specimens together with the average grain size, grain size range, and zirconia phase content are summarized in Table III. Apparently, as expected, hardness increases with the relative density. It can also be seen that while the alumina grain size in the ATZ-1 specimen remained similar to its original value (0.7 μm), that of the zirconia was drastically reduced (0.37 μm). The explanation is that the lower hardness of zirconia makes for more effective granulation during ball milling. Moreover, the porous nature of this specimen hinders grain growth during sintering. This is confirmed by the fracture-surface SEM image (Fig. 7a), which shows the very fine grain structure associated with the porosities.

In the denser specimens, ATZ-3 and ZTA-4, normal as well as exaggerated grain growth was observed (Fig. 7b). It is seen that the low density of these specimens is a dominant factor in reducing bending strength and the t-phase volume fraction. ATZ composites of similar composition, prepared by sintering of co-precipitated powders [4], showed relative densities of 90% for 1400 °C, and 97.5% for 1650 °C sintering. Grain sizes were reported to be 0.60 and 1.8 μm, respectively.

Generally, the present ATZ specimens show bending strengths in the range of 250–500 MPa, which are lower compared to those reported for closely similar compositions isostatically pressed and sintered (1270–1340 MPa in [4]) or hot-pressed (1070 MPa in [26]). However, the ATZ-3 specimen has shown a significant improvement in fracture

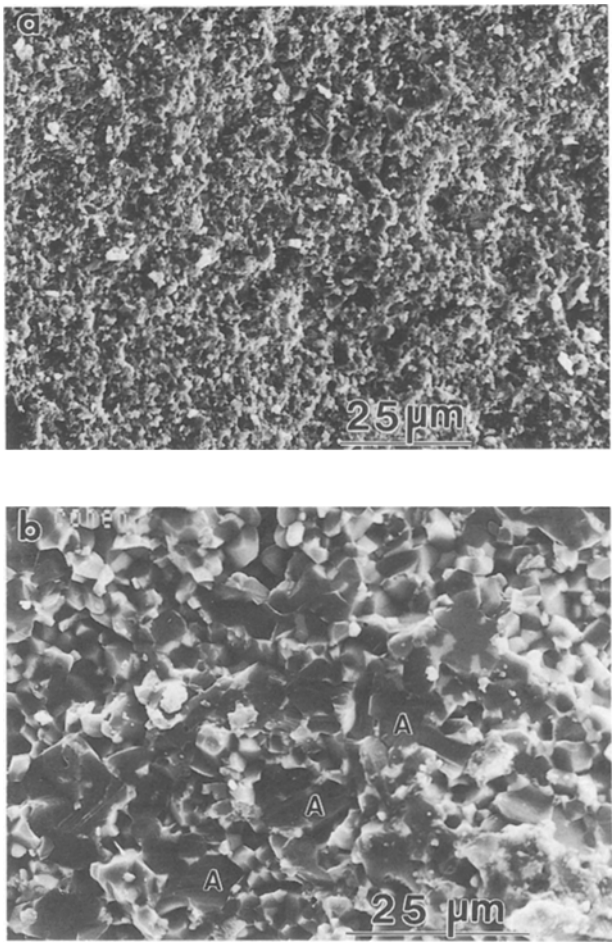

Figure 7 SEM images from the fracture surfaces of (a) ATZ-1 and (b) ZTA-4, showing the fine-grained porous microstructure in the former and the exaggerated alumina (A) grain growth in the latter.

toughness: 9 MPa $m^{1/2}$ compared to 4.5–5.8 MPa $m^{1/2}$ in [4], and 7 MPa $m^{1/2}$ in [26]. Because all these materials contained a high volume fraction of the t-phase (over 90%), the fracture toughness improvement is partly attributable to the differences in their relative densities: 96% compared to 96%–98% in [4] and 99.5% in [26]. It turns out that the higher the density (needed for retention of the t-phase through the matrix elastic constraint), the lower the probability of microcracks forming during cooling, due to lack of stress concentrators, this in turn reduces the contribution of the crack deflection toughening mechanism.

The improvement in fracture toughness in the present specimens is also attributable to the higher volume fraction of the t grains close to the critical size, determined by Green [14] to be about 0.7–0.8 μm for the 15–20 vol % ZrO_2 composition. Comparison of the t grain-size data in Table III with the reported data, shows that the specimen with highest fracture toughness (ATZ-3) has an average grain size of 0.91 μm, very close to the critical size values. By contrast, the t grain size in the corresponding specimens (1600 °C sintering) was larger both in [4] ($d \simeq 1.09$ μm) and in [26] ($d \simeq 1$ μm).

The ZTA-4 specimen shows higher hardness, apparently contributed by the high volume fraction of the alumina matrix. The relatively low bending strength is most probably due to the porosity of the composite.

Composites reported in the literature with closely similar composition, density and grain size [27, 28], showed comparable bending strength ($\simeq$ 300 MPa) but higher fracture toughness (5.5 compared to 7.3 MPa $m^{1/2}$). In this context it should be borne in mind that crosshead velocity is an important factor in bending strength measurement. The low velocity of 0.1 mm min^{-1} in the present work ensured a very conservative regime of slow crack growth, and made for lower but more reliable bending strength values.

The SENB fracture toughness results in the present study are generally far more conservative and representative of the bulk property, compared with the indentation tests. In conclusion, notable improvements were obtained, especially in the fracture toughness of the 96% dense ATZ specimens with critical t grain size.

Acknowledgements

The financial support of the Israel Ministry of Industry and Commerce under contract T/108/87 is acknowledged. The author thanks Mr E. Cohen for performing some of the experiments.

References

1. K. TSUKUMA, K. UEDA and M. SHIMADA, *J. Amer. Ceram. Soc.* **68** (1985) C-4.
2. F. F. LANGE, *ibid.* **66** (1983) 396.
3. J. WANG and R. STEVENS, *J. Mater. Sci.* **23** (1988) 804.
4. S. RAJENDRAN, M. V. SWAIN and H. J. ROSSELL, *ibid.* **23** (1988) 1805.
5. J. WANG and R. STEVENS, *ibid.* **24** (1989) 3421.
6. F. F. LANGE, T. YAMAGUCHI, B. I. DAVIS and P. E. D. MORGAN, *J. Amer. Ceram. Soc.* **71** (1988) 446.
7. F. F. LANGE and M. M. HIRLINGER, *ibid.* **67** (1984) 164.
8. S. HORI, R. KURITA, M. YOSHIMURA and S. SOMIYA, *J. Mater. Sci. Lett.* **4** (1985) 1067.
9. J-T. LIN and H-Y. LU, *Ceram. Int.* **14** (1988) 251.
10. S. HORI, R. KURITA, M. YOSHIMURA and S. SOMIYA, in "Advances in Ceramics", Vol. 24A, edited by S. Somiya, N. Yamamoto and H. Hanagida (American Ceramic Society, Westerville, Ohio, 1988) p. 423.
11. M. KAGAWA, M. KIKUCHI, Y. SYONO and T. NAGAE, *J. Amer. Ceram. Soc.* **66** (1983) 751.
12. F. F. LANGE, *J. Mater. Sci.* **17** (1982) 225.
13. R. C. GARVIE and M. V. SWAIN, *ibid.* **20** (1985) 1193.
14. D. J. GREEN, *J. Amer. Ceram. Soc.* **65** (1982) 610.
15. M. RUHLE, N. CLAUSSEN and A. H. HEUER, *ibid.* **69** (1986) 195.
16. E. BISCHOFF and M. RUHLE, in "Advances in Ceramics", Vol. 24B, edited by S. Somiya, N. Yamamoto and H. Hanagida (American Ceramic Society, Westerville, Ohio, 1988) p. 635.
17. F. F. LANGE and M. METCALF, *J. Amer. Ceram. Soc.* **66** (1983) 398.
18. F. F. LANGE, B. I. DAVIS and I. A. AKSAY, *ibid.* **66** (1983) 407.
19. T. S. YEN and J. K. GUO, in "Advances in Ceramics", Vol. 24B, edited by S. Somiya, N. Yamamoto and H. Hanagida (American Ceramic Society, Westerville, Ohio, 1988) p. 573.
20. K. TSUKUMA, T. TAKAHATA and M. SHIOMI, *ibid.*, p. 721.
21. F. WAKAI, S. SAKAGUCHI and Y. MATSUNO, *Adv. Ceram. Mater.* **1** (1986) 259.
22. T. G. NIEH, C. M. McNALLY and J. WADSWORTH, *Scripta Metall.* **22** (1988) 1297.
23. *Idem, ibid.* **23** (1989) 457.
24. D. L. PORTER and A. H. HEUER, *J. Amer. Ceram. Soc.* **62** (1979) 298.
25. B. KIBBEL and A. H. HEUER, *ibid.* **69** (1986) 231.
26. F. F. LANGE, *J. Mater. Sci.* **17** (1982) 247.
27. G. DE PORTU, C. FIORI and O. SBAIZERO, in "Advances in Ceramics", Vol. 24B, edited by S. Somiya, N. Yamamoto and H. Hanagida (American Ceramic Society, Westerville, Ohio, 1988) p. 1063.
28. W. KLADNIG and G. GRITZNER, *J. Mater. Sci. Lett.* **6** (1987) 1235.

Received 16 July 1991
and accepted 10 January 1992